JM PAPERS

Cloaking waveguide defects at low frequencies using local wall deformations

Daria Zyla[1] 🄳 and **Tomasz Bobinski**[1] 🄳

[1]Institute of Aeronautics and Applied Mechanics, Warsaw University of Technology, 00-665 Warsaw, Poland
Corresponding author: Tomasz Bobinski, tomasz.bobinski@pw.edu.pl

We present a novel technique to render objects invisible to incident waves in a water waveguide system with parallel walls at low frequencies. The invisibility of a waveguide defect, specifically a vertical surface-piercing circular cylinder, is achieved through local deformations of the waveguide walls in the immediate vicinity of the defect. Our method results in a reflection coefficient that is at least 20 times lower than in the case of a parallel waveguide. The effect is observed over a broad frequency range. Experimental results confirm the high efficiency of our approach, showing that backscattered energy is reduced by a factor of 100–5000 compared with the reference case within the considered frequency range.

Key words: surface gravity waves, wave scattering

1. Introduction

Controlling water waves through interaction with specially designed structures is important in energy conversion and protection of off-shore constructions (Zhu *et al.* 2024). Efficient control of wave propagation can be achieved using materials structured at the subwavelength scale which exhibit unusual properties, known as metamaterials (Walser 2000). These materials have enabled the realization of the cloaking phenomenon, where the object becomes invisible to the incident wave regardless of the wave direction or frequency (Leonhardt 2006; Pendry, Schurig & Smith 2006). To effectively render an object invisible, a cloaking device must be both omnidirectional and broadband (Choi & Howell 2015).
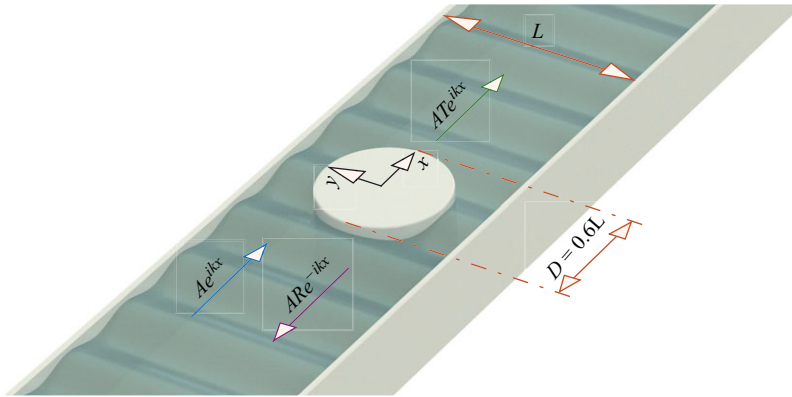
Figure 1. Water wave system. Parallel waveguide of width L and cylinder of diameter D in the plane of symmetry (Ae^{ikx} denotes incident wave, ARe^{-ikx} denotes reflected wave with reflection coefficient R and ATe^{ikx} is transmitted wave with transmission coefficient T).

The invisibility effect was initially confirmed experimentally for electromagnetic waves (Schurig *et al.* 2006). Thanks to the similarity of the equations governing the propagation of different types of waves, the cloaking phenomenon was achieved in the case of acoustic (Zigoneanu, Popa & Cummer 2014; Zaremanesh & Bahrami 2022), seismic (Brûlé *et al.* 2014) and water waves (Porter & Newman 2014). In the case of surface water waves, the invisibility effect can be obtained using different approaches. The first possibility is to design bathymetry around an object to be hidden (Porter & Newman 2014; Zareei & Alam 2015; Bobinski *et al.* 2018; Zou *et al.* 2019; Cen *et al.* 2024). The second method is based on the wave interaction with an array of structured objects piercing the free surface (Newman 2014; Dupont *et al.* 2016; Kucher *et al.* 2023). The third method involves altering free-surface boundary conditions by surrounding an object with an elastic composite plate that floats on the surface (Iida, Zareei & Alam 2023).

In this work, we focus on cloaking a defect within a water waveguide system, where strong scattering is typically observed. The defect is a vertical, surface-piercing cylinder located on the centreline (figure 1). Systems with a symmetrical defect about the centreline of the waveguide with parallel walls have been extensively analysed in the context of the existence of trapped modes (Callan, Linton & Evans 1991; Evans, Levitin & Vassiliev 1994; Evans & Porter 1997; Linton & McIver 2007; Cobelli *et al.* 2011). Trapped modes are localized solutions of the homogeneous wave equation with a real resonance frequency. They are characterized by finite energy rapidly decaying with the distance from the defect (Pagneux 2013). The eigenvalue associated with a trapped mode is embedded in the real continuous spectrum. Our work focuses on the background scattering produced by a symmetrical obstacle within this spectrum.

Here, we present a new approach to cloak an object at a low-frequency range. We show that by manipulating the local shape of the waveguide walls, one can significantly reduce the backscattering produced by a defect inside a waveguide. We design the shape of the wall perturbation through an optimization process and quantitatively confirm its broadband cloaking properties in the experiments. Section 2 presents the modelling and optimization problem with numerical results. The experimental results are presented in § 3.

2. Modelling and numerical results

We consider a system with linear surface water waves propagating within a parallel waveguide of width L characterized by a flat bottom and a surface-piercing cylinder of diameter D positioned at the plane of symmetry. The system is illustrated in figure 1. We assume a harmonic regime with deformation of the free surface expressed as $\zeta(x, y, t) = Re\{\eta(x, y) \cdot e^{-i\omega t}\}$, where η denotes the complex wavefield, ω is the frequency and Re denotes the real part of complex field.

2.1. *Governing equations*

In the analysed case, the propagation of waves can be described by the Helmholtz equation along with the Neumann boundary condition at the rigid walls of the waveguide, at $y = \pm L/2$, and the cylinder, at $x^2 + y^2 = D^2/4$

$$\Delta\eta(x, y) + k^2\eta(x, y) = 0, \tag{2.1}$$

$$\left.\frac{\partial\eta}{\partial\mathbf{n}}\right|_{walls} = 0, \tag{2.2}$$

with k being a wavenumber following the linear dispersion relation

$$\omega^2 = gk\tanh(kh), \tag{2.3}$$

where g represents the gravity constant, ω denotes frequency and h is the water depth. We restrict our considerations to the low-frequency range $kL/\pi < 1$, i.e. there is only one mode propagating. The solution in the far-field region of the cylinder can be expressed as

$$\eta(x) = \begin{cases} Ae^{ikx} + ARe^{-ikx}, & \text{in the region I,} \\ ATe^{ikx}, & \text{in the region II,} \end{cases} \tag{2.4}$$

where A denotes the amplitude of the incident wave and R and T denote the reflection and transmission coefficients, respectively. Region I corresponds to the far-field region in front of the cylinder $(x < 0)$, and region II corresponds to the far-field region behind the cylinder $(x > 0)$.

2.2. *Making defect invisible – framework*

We perform numerical simulations with a cylinder diameter of $D = 0.6L$ in a domain $x \in (-5, 5)L$. We solve the Helmholtz equation (2.1) using the finite element method implemented in MATLAB PDE Toolbox. We impose the Dirichlet boundary condition $\eta = 1$ at $x = -5L$ and radiation condition $\partial_x\eta = ik\eta$ at $x = 5L$. The maximum edge length of the mesh element is $h_{max}/L = 0.01$. It is worth noting that this problem can be solved using other methods, such as the method proposed by Kirby (2008) combining a wave-based modal solution with the finite element solution. The scattering of a cylinder within a parallel waveguide can be analysed using the multipole method proposed by Linton & Evans (1992). We verify the results obtained using the finite element method with the multipole method for this geometry. We also consider different domain sizes and confirm that the considered domain size $x \in (-5, 5)L$ is sufficient to provide accurate results.

The presence of the cylinder in the analysed scenario leads to a significant reflection of incident wave energy. In the case of a perfectly hidden object, there is no reflection $(R = 0)$, resulting in perfect transmission $(T = 1)$. We aim to make the cylinder invisible to incident waves by creating narrow indentations F in the waveguide walls near the obstacle. The walls are given by $y = \pm(L/2 + F)$. To determine the specific shape of the wall perturbation providing broadband reduction of the reflection coefficient, we minimize
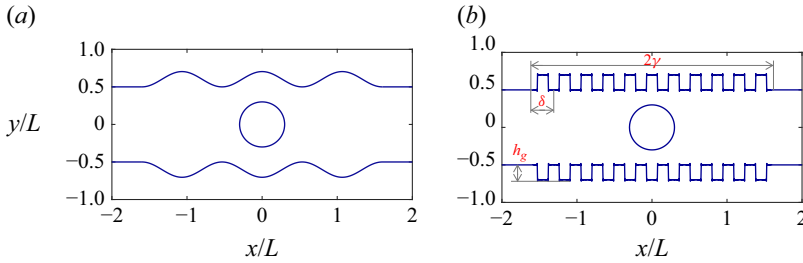
(a)

(b)

Figure 2. Examples of wall modifications considered in the optimization problem with the parameters defining the shape: (a) $h_g/L = 0.16$, $\gamma/L = 1.6$, $\delta/L = 1.06$, $N = 2$ and (b) $h_g/L = 0.2$, $\gamma/L = 1.6$, $\delta/L = 0.29$, $N = 60$.

the cloaking factor χ in the frequency range $k \in (k_1, k_2)$ with $k_1 = 0.01\pi/L$ and $k_2 = \pi/L$. The cloaking factor is defined as

$$\chi = \frac{\int_{k_1}^{k_2} |R|^2 \mathrm{d}k}{\int_{k_1}^{k_2} |R_0|^2 \mathrm{d}k}, \tag{2.5}$$

where R_0 denotes the reflection coefficient for the reference case with straight parallel walls. One has to notice that, due to energy conservation, minimizing the reflection coefficient results in the absolute value of the transmission coefficient being close to unity but does not guarantee that the phase shift in the transmitted wave is zero. As an alternative objective function, we consider minimization of the cloaking factor based on total scattered energy, which physically represents radiated power, defined in the following way:

$$\chi_{sc} = \frac{\int_{k_1}^{k_2} (|R|^2 + |T - 1|^2) \mathrm{d}k}{\int_{k_1}^{k_2} (|R_0|^2 + |T_0 - 1|^2) \mathrm{d}k}. \tag{2.6}$$

To minimize χ and χ_{sc}, we consider wall deformations that are symmetrical with respect to the cylinder. The variability of the walls near the obstacle is achieved through the utilization of a cosine Fourier series

$$F(h_g, \zeta, n, x) = \sum_{n=1}^{N} \frac{2h_g}{\pi(2n-1)} \left\{ \cos\left(\frac{\zeta\pi}{\gamma}(2n-1)x\right) - \cos\left(\zeta\pi(2n-1)\right) \right\} (-1)^{5n-1}, \tag{2.7}$$

$$\zeta = \begin{cases} \lfloor \frac{2\gamma}{\delta} \rfloor, & \mathrm{mod}\ (\lfloor \frac{2\gamma}{\delta} \rfloor, 2) \neq 0, \\ 1, & \mathrm{otherwise.} \end{cases} \tag{2.8}$$

In the above relation, h_g denotes the depth of the groove in the channel wall, γ represents half of the width of the variable geometry part, δ denotes the width of a single groove and $\lfloor 2\gamma/\delta \rfloor$ denotes the floor function. We impose constraints on the parameters defining wall deformation: (i) $1 \leq N \leq 60$, (ii) $0.09 \leq h_g/L \leq 1$, (iii) $0.2 \leq \delta/L \leq 4$ and (iv) $0.1 \leq \gamma/L \leq 2$. The constraint $\delta < 2\gamma$ is introduced to eliminate incorrect geometries. Figure 2 depicts examples of geometries considered in the optimization problem with a graphical representation of different parameters defining the geometry of waveguide indentations. The shape of indentations given by (2.7) is initially chosen due to the lack of knowledge about the expected optimal shape. Its definition is developed to ensure that a
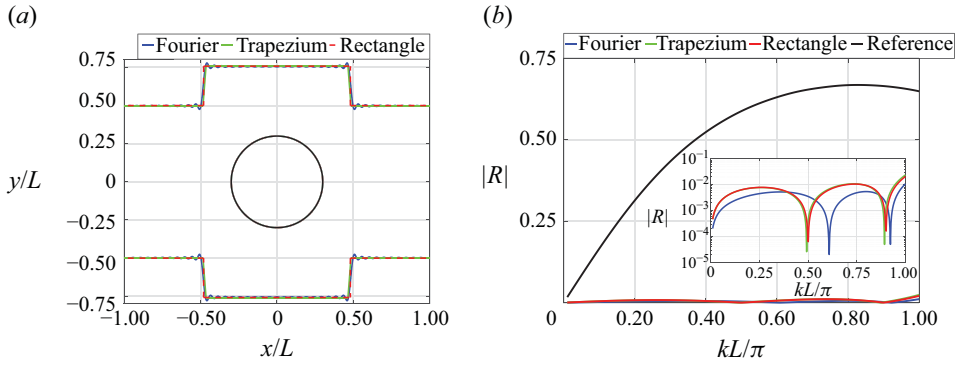
1006 A26-4

Figure 3. (*a*) Geometries providing cloaking phenomenon: Fourier series geometry (blue solid line, $h_g/L = 0.258$, $\delta/L = 1.93$, $\gamma/L = 0.97$, $N = 40$), trapezium (green solid line, $a/L = 0.485$, $b/L = 0.465$, $h_t/L = 0.26$) and rectangular geometry (red dashed line, $h_r/L = 0.26$, $w_r/L = 0.481$). (*b*) Reflection coefficient in the considered frequency range. The inset presents the reflection coefficient for three considered geometries in a logarithmic scale to show the difference in the results.

few parameters – such as the length of the region with variable geometry, depth, number of grooves and the shape of individual grooves – could unambiguously define the geometry of the grooved region. Additionally, continuity between the variable geometry region and the section with parallel waveguide walls is maintained.

The optimization process requires (i) mesh generation for a given set of parameters defining the wall shape perturbation, (ii) solving of the Helmholtz equation for the considered frequency range $kL/\pi \in (0.01, 1)$ and (iii) calculation of the cloaking factor χ. Given the lack of precise knowledge regarding the function $\chi(F)$ and the absence of analytical or derivative information, we employ a black box approach (Audet & Hare 2018). Considering the high computational cost of objective function evaluation, we use a surrogate-based method with a radial basis function approximation (Gutmann & Gutmann 2001; Vu *et al.* 2016). The initial guess is evaluated at 63 random points in the parametric space within the constrained values.

2.3. *Numerical results*

Minimizing the cloaking factor χ results in the geometry depicted in figure 3(*a*) by solid blue line (denoted as Fourier) with $\chi = 5.44 \times 10^{-5}$. The optimized shape resembles a trapezium, so we verify if we can simplify the indentation geometry and keep a similar objective function value. Geometry simplification is beneficial considering the manufacturing aspects of the experimental counterpart. Therefore, we repeat the optimization process, but this time, we vary the geometry by changing the height h_t and half of the lengths of both bases of an indentation a and b. As a result we obtain $\chi = 1.96 \cdot 10^{-4}$ for $a/L = 0.485$, $b/L = 0.465$ and $h_t/L = 0.26$ (figure 3*a* green solid line). The optimized trapezium has almost the same length of bases, so we go one step further with simplification, i.e. we perform optimization for a rectangular wall modification. We vary the height h_r and the half of the width w_r of the indentation. The best result is obtained for $h_r/L = 0.26$ and $w_r/L = 0.481$ with $\chi = 1.77 \cdot 10^{-4}$ (figure 3*a*, red dashed line). The efficiency of the rectangular geometry is shown in figure 4, where we present wave fields for $kL/\pi = 0.8253$ obtained for the reference case (parallel waveguide) and the waveguide with rectangular indentations. The comparison of the reflection coefficient in the considered frequency range for three considered wall modifications and
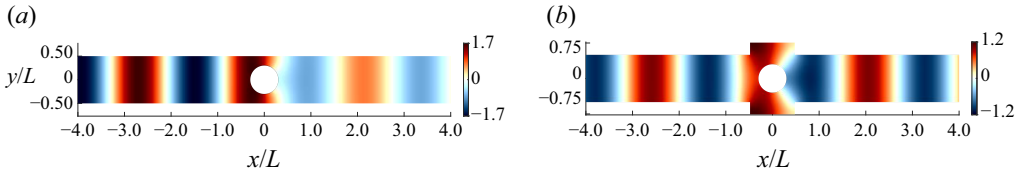
(*a*)

(*b*)

Figure 4. Numerical simulation. Real part of the wave fields for $kL/\pi = 0.8253$: (*a*) for a waveguide with parallel walls (reference case) and (*b*) with rectangular indentations. Wave fields are normalized by the incident wave amplitude.

the reference case is presented in figure 3(*b*), where a significant backscattering reduction is visible. The local minima of the reflection coefficient correspond to the resonant frequencies of a given system. In the case of rectangular indentations, they are observed for $kL/\pi \approx 0.5$ and $kL/\pi \approx 0.9$.

We perform the same analysis in the case of cloaking factor χ_{sc} (2.6) for three different geometries of the indentations, i.e. Fourier, trapezium and rectangular. The minimum value of χ_{sc} is obtained for the geometry defined through the Fourier series (2.7) with $\chi_{sc} = 0.239$. In the trapezium case, we obtain $\chi_{sc} = 0.24$ and for the rectangle $\chi_{sc} = 0.319$. Optimization of the cloaking factor based on total scattered energy provides slightly better results compared with optimization of χ in terms of the phase difference ($\Delta\varphi = \arg T$), where the phase shift is below 0.15π. The optimization of χ results in a phase shift below $\Delta\varphi \approx 0.25\pi$ in the considered frequency range. Unfortunately, in the case of minimizing χ_{sc}, the backscattered energy is much higher (see Appendix A for details), so we decided to perform experiments with the geometry provided by the minimization of χ.

The presented results are based on the initial choice of the function F, given by (2.7), which defines the shape of the indentations. It is worth noting that other choices of F might yield even better results with respect to the cloaking factors χ and χ_{sc}.

2.3.1. *Wave drift force*

For surface water waves, a cloaking device modifies not only scattered field but also the forces acting on an object. Cloaking an object should significantly reduce the force incident waves exert on the body. The force acting on a fixed body can be determined by integrating the pressure on the body's surface

$$\boldsymbol{F}(t) = \int_S \rho \left(\frac{\partial \Phi}{\partial t} + gz + \frac{1}{2}(\nabla\Phi)^2 \right) \boldsymbol{n}_S \mathrm{d}S, \tag{2.9}$$

with Φ being the velocity potential. We can decompose $\boldsymbol{F}(t)$ into a sum of first-order and second-order components. The second-order term has a fluctuating part at frequency 2ω and a time-independent wave drift force $\overline{\boldsymbol{F}^{(2)}}$, which can be expressed as

$$\overline{\boldsymbol{F}^{(2)}} = \frac{1}{T} \int_0^T \left(-\frac{1}{2}\rho g \int_{z=0} \left(\eta^{(1)} \right)^2 \cdot \boldsymbol{n}_s \mathrm{d}\ell + \frac{1}{2}\rho \int_S \left(\nabla\Phi^{(1)} \right)^2 \cdot \boldsymbol{n}_s \mathrm{d}S \right) \mathrm{d}t, \tag{2.10}$$

where S is the wetted body's surface, $\boldsymbol{n}_s$ denotes the unit normal vector and $\mathrm{d}\ell$ represents an infinitesimal segment along the water contour at $z = 0$ (Dupont *et al.* 2016). The first-order surface elevation is denoted as $\eta^{(1)}(x, y, t) = \mathrm{Re}\{\eta(x, y) \cdot e^{-i\omega t}\}$ and $\Phi^{(1)} = \Phi^{(1)}(x, y, z, t)$ denotes the first-order velocity potential expressed as

$$\Phi^{(1)}(x, y, z, t) = \mathrm{Re} \left(\frac{g}{i \cdot \omega} \cdot \eta(x, y) \cdot \frac{\cosh(k(z + h))}{\cosh(kh)} \cdot e^{-i\omega t} \right). \tag{2.11}$$
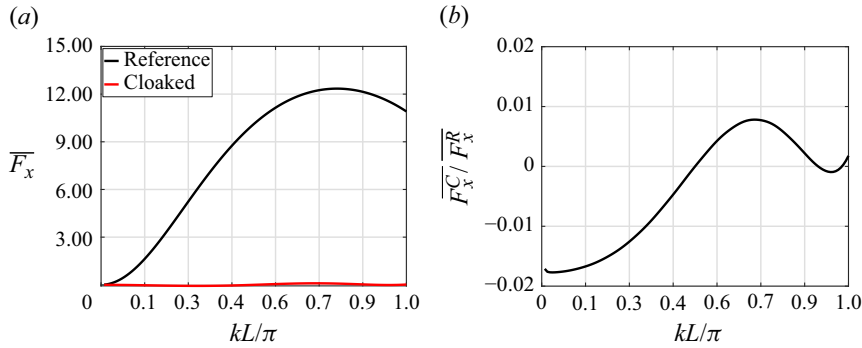
1006 A26-6

Figure 5. The mean drift force as a function of frequency kL/π: (*a*) the distribution of the mean horizontal force acting on the cylinder for the reference case and the cloaked case, respectively; (*b*) the ratio of the mean horizontal forces $\overline{F_x^C}/\overline{F_x^R}$, where $\overline{F_x^C}$ represents force for the cloaked case and $\overline{F_x^R}$ refers to the reference case with parallel walls.

We evaluate the mean drift force acting on the cylinder in the presence of waveguide wall indentations providing invisibility and compare the results with the reference geometry. We analyse the influence of rectangular indentations provided by the minimization of the cloaking factor χ. The results concerning the horizontal component of the drift force are presented for the two cases in figure 5(*a*). The black and red solid lines correspond to the force acting on a cylinder in a parallel waveguide $(\overline{F_X^R})$ and with rectangular indentations in the waveguide walls $(\overline{F_X^C})$, respectively. Implementing our cloaking device significantly reduces the horizontal force acting on the surface-piercing cylinder in the entire considered frequency range, with the maximum force being less than 2% of the force in the reference case (see figure 5*b*).

2.3.2. *Limitations of the cloaking device*

Any passive cloaking device designed to achieve invisibility within a specific frequency range does so at the cost of increased scattering outside this range (Monticone & Alù 2016). Our study focuses on optimizing waveguide wall indentations to reduce backscattering within the frequency range $kL/\pi \in (0.01, 1)$. To evaluate the performance of this system, we analyse its scattering behaviour outside the optimized frequency band, specifically in the range $kL/\pi \in (1, 2)$. Figure 6 compares the reflection coefficients of a cylinder in a waveguide with straight parallel walls (reference case, black solid line) and a cloaking geometry featuring rectangular wall indentations (red line). In the reference case, the reflection coefficient decreases initially, reaching resonance at $kL/\pi = 1.63$, before increasing with frequency. For the cloaking geometry, the reflection coefficient is significantly reduced up to $kL/\pi = 1.57$. Beyond this frequency, however, the reflection coefficient rises sharply, exceeding that of the reference case.

Extending the frequency range over which a cloaking device effectively minimizes scattering is a possibility that requires further investigation. Achieving a broader cloaking bandwidth would likely come at the cost of an increased cloaking factor χ (Monticone & Alù 2016).

Our cloaking device, consisting of indentations in the waveguide walls, is obtained through an optimization procedure based on the model of linear water waves. It is, therefore, important to consider the potential response of this system to nonlinear waves.
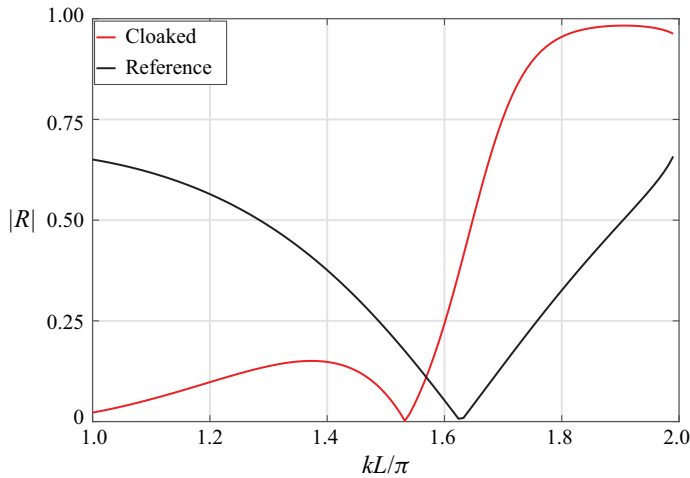
Figure 6. Reflection coefficient as a function of frequency for a cylinder in the waveguide with straight parallel walls (reference case) and cloaked case (with rectangular indentations).

In the weakly nonlinear regime, neglecting the forcing by the fundamental frequency (ω), the harmonics satisfy the Helmholtz equations (Belibassakis & Athanassoulis 2011)

$$\left(\Delta + k_n^2\right)\hat{\eta}_n(x, y) = 0, \tag{2.12}$$

where k_n is associated with $n\omega$, i.e. $D(n\omega, k_n) = 0$, where $D(\omega, k) = \omega^2 - gk\tanh(kh)$ denotes the water wave dispersion relation. A harmonic that satisfies (2.12) is called a free wave, whereas a non-dispersive term, with a wavenumber nk_1, being slaved to fundamental frequency is called a bound wave (Monsalve *et al.* 2022). For a cloaking geometry and waves with a fundamental frequency ω such that associated k is in the range $kL/\pi \in (0, 1)$, the first-order reflection coefficient is very low. Based on the results presented in figure 6, we expect that backscattering of the free wave component k_2 (associated with 2ω) will also be low for $k_2L/\pi < 1.57$ with the cloaking geometry, but for $k_2L/\pi > 1.57$ the reflection of this component would significantly increase. Given that the energy content of the fundamental frequency typically dominates the total energy, our cloaking device is expected to perform very well even for nonlinear waves within the considered frequency band. Nevertheless, the increased scattering of harmonic components outside this band highlights a limitation that could be addressed in future designs.

3. Experimental realization

Figure 7 illustrates a scheme of the employed measurement set-up, which consists of (i) a channel guiding surface water waves of total length 2.81 m, (ii) a wavemaker with a digitally controlled LinMot linear motor, (iii) a cylindrical obstacle, (iv) an absorbing beach minimizing spurious reflection from the end of the channel, (v) a light source and (vi) two cameras (BASLER ACA 2040-120um and BASLER ACA 1920-40um) allowing registration of a dot pattern placed in front and behind the cylinder. The average signal-to-noise ratio values, calculated based on (Gonzalez & Woods 2008) for these cameras, are 37.49 and 41.21 dB, respectively. The still water level h is $0.02 \pm 5 \times 10^{-4}$ m, the waveguide width is $L = 0.16$ m and the obstacle diameter $D = 0.6L = 0.096$ m. We analyse two waveguide geometries. The first one is a reference case with straight parallel
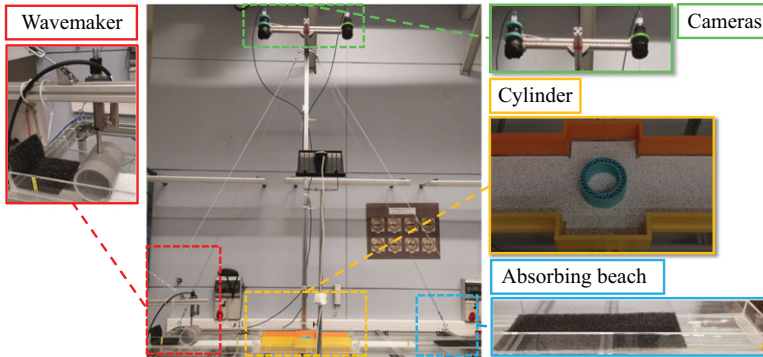
Figure 7. Experimental set-up consists of (i) a channel of length 2.81 m, (ii) a wavemaker – a cylindrical surface mounted to a linear motor, (iii) a cylindrical obstacle, (iv) an absorbing beach reducing reflection from the end of the channel, (v) a light source and (vi) two cameras (BASLER ACA 2040-120um and BASLER ACA 1920-40um).

walls. The second waveguide contains rectangular wall indentations ($h_r = 0.042$ m, $w_r = 0.077$ m). We generate surface waves employing a LinMot linear motor in the frequency range of 0.65 Hz to 1.36 Hz corresponding to $kL/\pi \in (0.53, 0.97)$. We conduct measurements for a duration corresponding to 20 time periods of oscillation.

3.1. *Measurement method*

We perform the measurements using a combination of the optical flow (OF) technique (Farnebäck 2003) and the synthetic schlieren (SS) technique (Moisy, Rabaud & Salsac 2009). The OF method enables the extraction of displacements from a reference image (e.g., dots), whereas the SS method transforms these displacements into deformations of the free water surface (Bheeroo & Mandel 2023). The SS method assumes certain geometrical approximations and, as a result, has a few limitations (Metzmacher *et al.* 2022): (i) weak amplitudes, (ii) weak slopes and (iii) weak paraxial angles. The distance between our cameras and the dot pattern placed on the bottom of the channel is 2.39 m, resulting in a maximum parallax angle of $\beta_{max} = 0.22$. In the considered frequency range, the amplitude of the generated waves is in the range of $A \in (0.39, 0.94)$ mm with the corresponding wave steepness in the range of $kA \in (4.76 \times 10^{-3}, 13.85 \times 10^{-3})$. The error in free-surface deformation reconstructions can be estimated as (Moisy *et al.* 2009)

$$\frac{\Delta \eta}{\eta_{rms}} = (5.0 \pm 0.2)\frac{L}{\lambda}\frac{\epsilon}{N_p},\tag{3.1}$$

with ϵ being relative Gaussian noise, λ being wavelength and $\eta_{rms} = A/\sqrt{2}$ for a sinusoidal wave, where *rms* is the root-mean-square. In our system, the error for the first camera is in the range 0.07×10^{-3} to 0.23×10^{-3}, while for the second camera, the error ranges from 0.08×10^{-3} to 0.26×10^{-3}.

3.2. *Experimental results*

Based on the obtained temporal evolution of the free-surface deformations, we extract wave fields using the Fourier transform in the time domain

$$\hat{\eta}_n(x, y, \omega) = \frac{2}{T_p}\int_{T_p}\eta(x, y, t)e^{in\omega t}\mathrm{d}t,\tag{3.2}$$
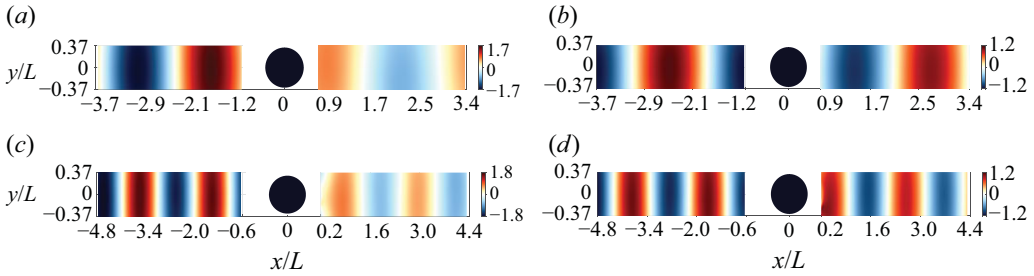
Figure 8. Real part of the experimental fields $\hat{\eta}_1(x, y)$ for parallel waveguide (*a* for $kL/\pi \approx 0.79$ and *c* for $kL/\pi \approx 0.94$) and rectangular cloaking geometry (*b* for $kL/\pi \approx 0.79$ and *d* for $kL/\pi \approx 0.94$). Wave fields are normalized by the incident wave amplitude.
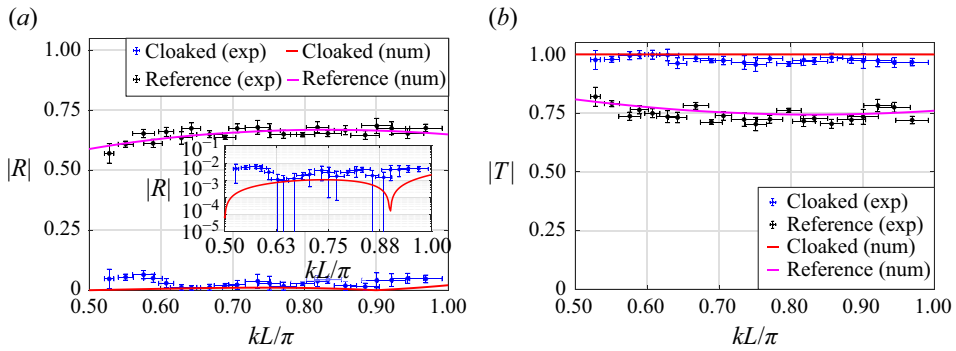

Figure 9. Comparison of numerical and experimental results. Reflection $|R|$ and transmission $|T|$ coefficients as a function of frequency kL/π. Black markers (experiment) and solid magenta lines (numerical simulation) correspond to the reference waveguide with straight walls. Blue markers (experiment) and red solid lines (numerical simulation) correspond to the waveguide with modified walls.

with ω being the fundamental frequency with $T_p = 2\pi/\omega$. An example of a wave field $Re(\hat{\eta}_1(x, y))$ is shown in figure 8 where, for the reference case (figure 8a,c), strong reflection is observed in front of the cylinder and a decrease in the wave amplitude behind the obstacle. The corresponding wave fields obtained in the case of the rectangular cloaking geometry are presented in figure 8(b,d). Based on wave field $\hat{\eta}_n(x, y)$, we extract transverse modes by projecting it onto $\phi_n(y) = \sqrt{(2 - \delta_{0n})/L} \cos(n\pi y/L)$

$$\eta_n(x) = \int_0^L \hat{\eta}_n(x, y)\sqrt{(2 - \delta_{0n})/L} \cos(n\pi y/L)\mathrm{d}y. \tag{3.3}$$

In the considered frequency range, only the plane mode propagates. This fact allows us to extract reflection R and transmission T coefficients using (2.4) (taking into account reflection from the end of the channel). In figure 9, we present a comparison of both coefficients as a function of kL/π for numerical simulations and experimental values. The error bars for the coefficients were estimated based on four realizations of the experiment at a 95 % confidence level and expressed as $\overline{|R|} \pm t_{(n-1,1-\alpha/2)}s/\sqrt{n}$ (similarly $\overline{|T|}$) with n, $\overline{|R|}$, s being the number of realizations, sample mean and sample standard deviation of the

results, respectively (Martin 2012). The $t_{(n-1,1-\alpha/2)}$ parameter is the critical value of the Student's t distribution for significance level $\alpha = 0.05$. We observe a significant reduction of the reflection coefficient in the entire frequency range. In the inset of figure 9, we present the same reflection coefficient in logarithmic scale to demonstrate the extremely high efficiency of the proposed cloaking device. Although the experimental values are not as good as in numerical simulations, one can notice that the reflection coefficient decreases by at least ten times the reference value corresponding to the straight parallel waveguide, meaning that, in the investigated frequency range, the energy of the reflected wave, proportional to $|R|^2$, is at least a hundred times lower than initially. The best experimental result is obtained for $kL/\pi \approx 0.64$, where backscattered energy is around 5000 times lower than in the reference case.

4. Conclusions

In this work, we present a novel technique for achieving an invisibility effect in a water wave system with a circular cylinder placed at the plane of symmetry of a parallel waveguide. Confinement of the considered system and the low-frequency range allow us to treat the problem as one-dimensional in the far field. We obtain the cloaking phenomenon by considering local deformations of the waveguide walls. The effect is visible in a broad range of frequencies. Wall deformation needs to be localized in the neighbourhood of the defect and adjusted for a given shape of an obstacle, suggesting our cloak belongs to a class of devices based on scattering cancellation (Fleury & Alu 2014). In numerical simulations, the reflection coefficient for the waveguide with the rectangular indentations is at least 20 times lower than that of the reference case with parallel waveguide walls in the entire frequency range. We confirm the high efficiency of the proposed technique experimentally, where the energy of the reflected wave is at least 100 times lower than in the reference case in the investigated frequency range.

Declaration of interests. The authors report no conflict of interest.

Data availability statement. The data that support the findings of this study are openly available in RepOD at https://doi.org/10.18150/PRNRHW.

Appendix A.

In this section, we present results concerning the minimization of the total scattered energy. The optimization of the cloaking factor χ_{sc} leads to the geometries presented in figure 10(*a*). The reflection coefficients corresponding to the geometries defined through Fourier series, trapezium and rectangle are presented in figure 10(*b*) by blue, green and red solid lines, respectively. In figure 10(*c*), we present the phase shift $\Delta\varphi$ for the two optimizations, where the top and the bottom figures correspond to the optimization of χ and χ_{sc}, respectively. The phase shift is non-zero in both optimization cases and is lower for χ_{sc}. However, the reflection coefficient is significantly higher than that obtained in the minimization process of χ. Geometry providing the lowest value of χ results in $\chi_{sc} = 0.4$. To sum up, we can obtain a significant difference in the reflection coefficient at the cost of an increase in phase shift.
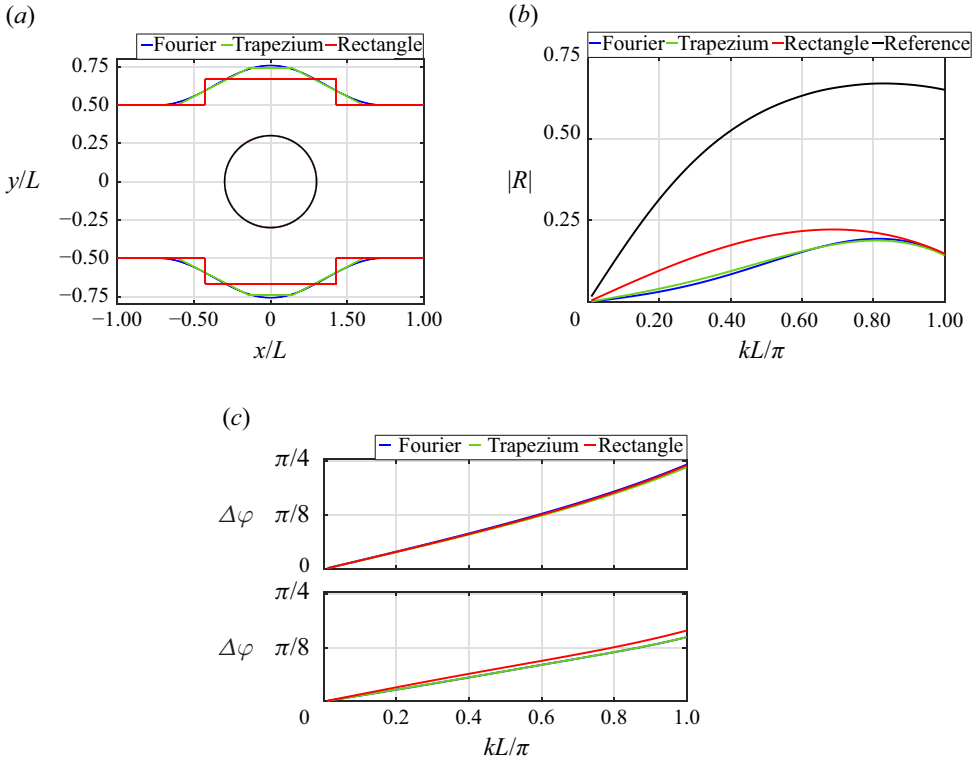
(*a*)

(*b*)

(*c*)

Figure 10. Optimization of the cloaking factor χ_{sc}: (*a*) comparison of the resulting geometries, (*b*) reflection coefficient as a function of frequency kL/π and (*c*) phase shift $\Delta\varphi$ for two optimizations (top: optimization of χ and bottom: optimization of χ_{sc}). The geometries of indentations providing the minimum value of χ_{sc} have the following dimensions: (i) Fourier ($h_g/L = 0.2024$, $\delta/L = 1.4405$, $\gamma/L = 0.7281$, $N = 2$), (ii) trapezium ($a/L = 0.606$, $b/L = 0.1458$, $h_t/L = 0.2391$), (iii) rectangle ($h_r/L = 0.1694$, $w_r/L = 0.4286$).
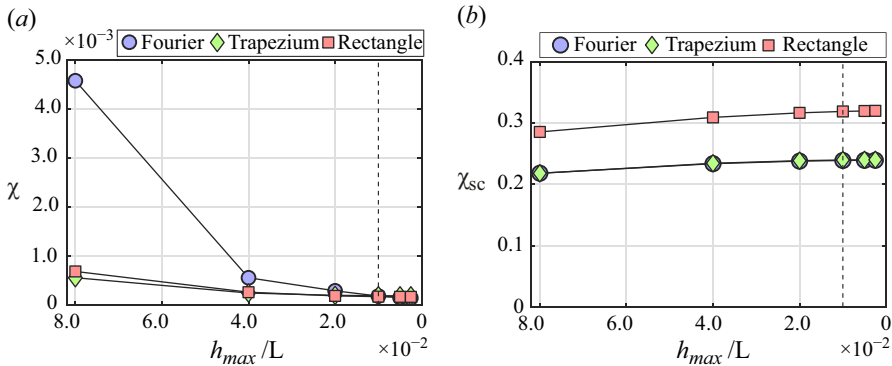
(*a*)

(*b*)

Figure 11. The influence of mesh element size on the cloaking factor (*a*) χ and (*b*) χ_{sc} value for three considered geometries. The vertical dashed line corresponds to the mesh size employed in the optimization, i.e. $h_{max}/L = 0.01$.

To verify the numerical results, we perform a mesh grid independence study by changing the maximum size of a single finite element. The largest size of finite element h_{max}/L is selected to ensure a minimum of 20 elements per wavelength. We successively decrease the element size and determine the corresponding cloaking factor χ and χ_{sc}. The results are presented in figure 11. The objective function χ values for $h_{max}/L = 0.01$ do not significantly differ from those obtained for lower values of h_{max}/L. We conclude that sufficient convergence is achieved for $h_{max}/L = 0.01$ in both optimization processes.

REFERENCES

AUDET, C. & HARE, W. 2018 *Derivative-Free and Blackbox Optimization*. Springer International Publishing.

BELIBASSAKIS, K. & ATHANASSOULIS, G. 2011 A coupled-mode system with application to nonlinear water waves propagating in finite water depth and in variable bathymetry regions. *Coast. Engng* **58** (4), 337–350.

BHEEROO, V. & MANDEL, T. 2023 Comparison of schlieren-based techniques for measurements of a turbulent and wavy free surface. *Exp. Fluids* **64** (6), 114.

BOBINSKI, T., MAUREL, A., PETITJEANS, P. & PAGNEUX, V. 2018 Backscattering reduction for resonating obstacle in water-wave channel. *J. Fluid Mech.* **845**, R4.

BRÛLÉ, S., JAVELAUD, E., ENOCH, S. & GUENNEAU, S. 2014 Experiments on seismic metamaterials: molding surface waves. *Phys. Rev. Lett.* **112** (13), 133901.

CALLAN, M., LINTON, C. & EVANS, D. 1991 Trapped modes in two-dimensional waveguides. *J. Fluid Mech.* **229** (1), 51.

CEN, Y., LIANG, D., CHENG, Q., LIU, X. & ZOU, S. 2024 Hydrodynamic performance of shallow-water waveguides subject to nonlinear waves. *Phys. Fluids* **36** (4), 047108.

CHOI, J.S. & HOWELL, J.C. 2015 Paraxial full-field cloaking. *Opt. Express* **23** (12), 15857.

COBELLI, P., PAGNEUX, V., MAUREL, A. & PETITJEANS, P. 2011 Experimental study on water-wave trapped modes. *J. Fluid Mech.* **666**, 445–476.

DUPONT, G., GUENNEAU, S., KIMMOUN, O., MOLIN, B. & ENOCH, S. 2016 Cloaking a vertical cylinder via homogenization in the mild-slope equation. *J. Fluid Mech.* **796**, R1.

EVANS, D., LEVITIN, M. & VASSILIEV, D. 1994 Existence theorems for trapped modes. *J. Fluid Mech.* **261**, 21–31.

EVANS, D. & PORTER, R. 1997 Trapped modes about multiple cylinders in a channel. *J. Fluid Mech.* **339**, 331–356.

FARNEBÄCK, G. 2003 Two-frame motion estimation based on polynomial expansion, In *Image Analysis: 13th Scandinavian Conference, SCIA 2003 Halmstad, Sweden, June 29–July 2, 2003 Proceedings 13*, pp. 363–370. Springer.

FLEURY, R. & ALU, A. 2014 Cloaking and invisibility: a review (invited review). *Prog. Electromagn. Res.* **147**, 171–202.

GONZALEZ, R.C. & WOODS, R.E. 2008 *Digital Image Processing*. Prentice Hall.

GUTMANN, H.-M. & GUTMANN, H.-M. 2001 A radial basis function method for global optimization. *J. Global Optim.* **19** (3), 201–227.

IIDA, T., ZAREEI, A. & ALAM, M.-R. 2023 Water wave cloaking using a floating composite plate. *J. Fluid Mech.* **954**, A4.

KIRBY, R. 2008 Modeling sound propagation in acoustic waveguides using a hybrid numerical method. *J. Acoust. Soc. Am.* **124** (4), 1930–1940.

KUCHER, S., KOŹLUK, A., PETITJEANS, P., MAUREL, A. & PAGNEUX, V. 2023 Backscattering reduction in a sharply bent water wave channel. *Phys. Rev. B* **108** (21), 214311.

LEONHARDT, U. 2006 Optical conformal mapping. *Science* **312** (5781), 1777–1780.

LINTON, C. & EVANS, D. 1992 The radiation and scattering of surface waves by a vertical circular cylinder in a channel. *Phil. Trans. R. Soc. Lond. A: Phys. Engng Sci.* **338** (1650), 325–357.

LINTON, C. & MCIVER, P. 2007 Embedded trapped modes in water waves and acoustics. *Wave Motion* **45** (1–2), 16–29.

MARTIN, B. 2012 *Statistics for Physical Sciences: An Introduction*. Academic Press.

METZMACHER, J., LAGUBEAU, G., POTY, M. & VANDEWALLE, N. 2022 Double pattern improves the Schlieren methods for measuring liquid–air interface topography. *Exp. Fluids* **63** (8), 120.

MOISY, F., RABAUD, M. & SALSAC, K. 2009 A synthetic Schlieren method for the measurement of the topography of a liquid interface. *Exp. Fluids* **46** (6), 1021–1036.

MONSALVE, E., MAUREL, A., PAGNEUX, V. & PETITJEANS, P. 2022 Nonlinear waves passing over rectangular obstacles: multimodal method and experimental validation. *Fluids* **7** (5), 145.

MONTICONE, F. & ALÙ, A. 2016 Invisibility exposed: physical bounds on passive cloaking. *Optica* **3** (7), 718–724.

NEWMAN, J. 2014 Cloaking a circular cylinder in water waves. *Eur. J. Mech. B/Fluids* **47**, 145–150.

PAGNEUX, V. 2013 *Trapped Modes and Edge Resonances in Acoustics and Elasticity*. Springer Vienna.

PENDRY, J., SCHURIG, D. & SMITH, D. 2006 Controlling electromagnetic fields. *Science* **312** (5781), 1780–1782.

PORTER, R. & NEWMAN, J. 2014 Cloaking of a vertical cylinder in waves using variable bathymetry. *J. Fluid Mech.* **750**, 124–143.

SCHURIG, D., MOCK, J., JUSTICE, B., CUMMER, S., PENDRY, J., STARR, A. & SMITH, D. 2006 Metamaterial electromagnetic cloak at microwave frequencies. *Science* **314** (5801), 977–980.

VU, K. K., D'AMBROSIO, C., HAMADI, Y. & LIBERTI, L. 2016 Surrogate-based methods for black-box optimization. *Intl Trans. Oper. Res.* **24** (3), 393–424.

WALSER, R. M. 2000 Metamaterials: What are they? What are they good for? In *APS March Meeting Abstracts*, pp. Z5.001. American Physical Society.

ZAREEI, A. & ALAM, M.-R. 2015 Cloaking in shallow-water waves via nonlinear medium transformation. *J. Fluid Mech.* **778**, 273–287.

ZAREMANESH, M. & BAHRAMI, A. 2022 Multilayer acoustic invisibility cloak based on composite lattice. *Sci. Rep.-UK* **12** (1), 16096.

ZHU, S., ZHAO, X., HAN, L., ZI, J., HU, X. & CHEN, H. 2024 Controlling water waves with artificial structures. *Nat. Rev. Phys.* **6** (4), 231–245.

ZIGONEANU, L., POPA, B.-I. & CUMMER, S. A. 2014 Three-dimensional broadband omnidirectional acoustic ground cloak. *Nat. Mater.* **13** (4), 352–355.

ZOU, S., XU, Y., ZATIANINA, R., LI, C., LIANG, X., ZHU, L., ZHANG, Y., LIU, G., LIU, Q.H., CHEN, H. & WANG, Z. 2019 Broadband waveguide cloak for water waves. *Phys. Rev. Lett.* **123** (7), 074501.